Journal of Controlled Release 220 (2015) 484–494

Contents lists available at ScienceDirect

Journal of Controlled Release

journal homepage: www.elsevier.com/locate/jconrel

Porphyrin-phospholipid liposomes with tunable leakiness

Dandan Luo [a], Kevin A. Carter [a], Aida Razi [b], Jumin Geng [a], Shuai Shao [a], Cuiyan Lin [a], Joaquin Ortega [b], Jonathan F. Lovell [a,*]

[a] Department of Biomedical Engineering, University at Buffalo, State University of New York, Buffalo, NY 14260, USA
[b] Department of Biochemistry and Biomedical Sciences and M. G. DeGroote Institute for Infectious Diseases Research, McMaster University, Hamilton, ON L8S4L8, Canada

ARTICLE INFO

Article history:
Received 10 August 2015
Received in revised form 6 November 2015
Accepted 10 November 2015
Available online 11 November 2015

Keywords:
Liposomes
Photodynamic therapy
Porphyrin
Doxorubicin
Vasculature
Cancer

ABSTRACT

Drug bioavailability is a key consideration for drug delivery systems. When loaded with doxorubicin, liposomes containing 5 molar % porphyrin-phospholipid (HPPH liposomes) exhibited *in vitro* and *in vivo* serum stability that could be fine-tuned by varying the drug-to-lipid ratio. A higher drug loading ratio destabilized the liposomes, in contrast to standard liposomes which displayed an opposite and less pronounced trend. Following systemic administration of HPPH liposomes, near infrared laser irradiation induced vascular photodynamic damage, resulting in enhanced liposomal doxorubicin accumulation in tumors. In laser-irradiated tumors, the use of leaky HPPH liposomes resulted in improved doxorubicin bioavailability compared to stable standard liposomes. Using this approach, a single photo-treatment with 10 mg/kg doxorubicin rapidly eradicated tumors in athymic nude mice bearing KB or MIA Paca-2 xenografts.

1. Introduction

Liposomes are self-assembled, lipid-based nanocarriers that are used clinically for drug delivery [1–3]. Long-circulating liposomal doxorubicin (Dox) has been approved for treatment of various cancers [4]. Despite enhanced intratumoral deposition, the clinical efficacy of long-circulating liposomal Dox is not necessarily superior to that of free Dox [5,6] while the main benefit is reduced cardiotoxicity compared to the free drug [6]. Slow drug release from the carrier reduces bioavailability and efficacy [7]. PEGylated liposomes tend to produce greater tumoral drug deposition due to their longer circulation times [8–10]. However, to become bioavailable, the encapsulated drug needs to be released from the carrier. Drugs loaded in stable and long-circulating liposomes remain partially entrapped and inactive after extravasation into the tumor [11].

Numerous strategies have been proposed to improve drug bioavailability from liposomes and other nanocarriers [12]. These include pH-sensitive liposomes [13,14], heat sensitive liposomes [15,16] and enzymatic responsive liposomes [17], all of which release their content in response to local physiological or externally applied stimuli. An alternative and more generalized approach is to design liposomes with a faster drug release rate. This strategy has been demonstrated with liposomal mitoxantrone, where shorter-circulating formulations showed therapeutic advantages over more stable, longer-circulating ones [18–20]. Varying the drug to lipid ratio has been proposed as a simple way of potentially controlling the rates of drug release [21–23]. Here, a faster-releasing and shorter-circulating liposome system is explored which exhibits enhanced bioavailability and therapeutic efficacy following tumor vasculature permeabilization.

Vascular barriers and heterogeneous drug distribution are central challenges for delivery of nanoparticulate chemotherapeutics to solid tumors [24]. Despite the endothelial defects found in growing tumor blood vessels, the enhanced permeability and retention (EPR) effect alone is less than ideal to enable sufficient nanoparticle extravasation for tumor eradication and additional strategies can be beneficial [25–27].

Photodynamic therapy (PDT) can be used to permeabilize tumor vasculature, although it can also induce thrombus formation and blood flow stasis [28]. PDT generates singlet oxygen, which can damage vascular endothelial cells and induce the formation of endothelial intercellular gaps, resulting in leakier tumor microvasculature and an augmented EPR effect [29,30]. PDT enhances liposomal drug delivery in mouse models of cancer in different scenarios using photosensitizers that: 1) extravasate to the tumor after leaving circulation [31]; 2) remain in blood circulation for vascular PDT [29]; and 3) are specifically targeted to tumor neovasculature [32].

2-[1-hexyloxyethyl]-2-devinyl pyropheophorbide-a (HPPH) is a second generation photosensitizer under clinical evaluation as a PDT agent [33]. Our group previously conjugated HPPH to a lysophosphatidylcholine to generate a porphyrin-phospholipid (PoP) and incorporated it into liposomes which could then be permeabilized with near infrared light [34]. PoP has been used for a variety of purposes including light-triggered release of Dox, a handle for radionuclides for positron emission tomography, optical imaging, and a scaffold for simple peptide functionalization

* Corresponding author.
E-mail address: jflovell@buffalo.edu (J.F. Lovell).

http://dx.doi.org/10.1016/j.jconrel.2015.11.011
0168-3659/

of liposomes [35–38]. In this study, HPPH-lipid is used not for the effect of light-triggered drug release, but rather for two other purposes: 1) for serum-induced tunable Dox leakiness from liposomes and 2) for PDT-mediated tumor vasculature permeabilization. Relatively short-circulating, leaky formulations of Dox are shown to have superior anti-tumor efficacy following PDT-mediated tumor vasculature permeabilization.

2. Methods

2.1. Liposome preparation

Chemicals were obtained from Sigma unless noted otherwise. HPPH-lipid was synthesized as previously described [34]. HPPH liposome composition was 45 mol% 1,2-distearoyl-sn-glycero-3-phosphocholine (DSPC; Avanti #850365P), 45 mol% cholesterol (CHOL, Avanti #700000P), 5 mol% HPPH-lipid and 5 mol% 1,2-distearoyl-sn-glycero-3-phosphoethanolamine-N-[methoxy(polyethylene glycol)-2000] (DSPE-PEG2K; Avanti #880120P). Stable standard (std.) liposomes were composed of 50 mol% DSPC, 45 mol% cholesterol and 5 mol% DSPE-PEG2K. Unless stated otherwise, leaky HPPH liposomes and stable std. liposomes used a 1:4 drug: lipid (D:L) loading molar ratio. Lipids in the indicated molar ratios were fully dissolved in 2 mL ethanol at 70 °C, then 8 mL 250 mM ammonium sulfate (pH 5.5) buffer was injected to the lipid solution. The lipid solution was passed 10 times at 70 °C through a high pressure lipid extruder (Northern Lipids) with sequentially stacked polycarbonate membranes of 0.2, 0.1 and 0.08 μm pore size. Free ammonium sulfate was removed by dialysis in a 10% sucrose solution with 10 mM HEPES (pH 7.4). To prepare HPPH liposomes or std. liposomes, doxorubicin (LC Labs #D-4000) was then loaded by adding the indicated ratio of drug into liposome solutions and incubating at 60 °C for 1 h. Liposome sizes were determined in phosphate buffered saline (PBS) at room temperature by dynamic light scattering to be 89–96 nm for both HPPH liposomes and std. liposomes. Loading efficiency was determined by running 500 μL of liposomes diluted 10 times over a Sephadex G-75 column. 24 × 1 mL fractions were collected and the loading efficiency was determined as the percentage of the drugs in the liposome-containing fractions (which elute in the first 3–8 mL). Dox was measured using fluorescence with an excitation of 480 nm and emission of 590 nm.

2.2. Cryo-electron microscopy

Approximately 3.4 μL of stable std. liposomes (D:L molar ratio 1:4, ~20 mg/mL lipids), leaky HPPH liposomes (D:L molar ratio 1:4) or empty HPPH liposomes in buffer containing 10% sucrose and 10 mM histidine were deposited in holey carbon grids (c-flat CF-2/2-2C-T) prepared with an additional layer of continuous carbon ~5–10 nm thick. Grids were treated with glow discharge at 5 mA for 15 s before the liposome samples were deposited on them. The grids were then blotted and plunged in liquid ethane at −180 °C using a Vitrobot (FEI) with the blotting chamber maintained at 25 °C and 100% relative humidity. Liposomes were imaged in a JEOL2010F transmission electron microscope at 200 kV using a Gatan 914 cryo-holder. Images were recorded in SO-163 films and collected using a total dose of ~15–20 electrons per $Å^2$, magnification ×50,000 and a defocus that ranged between −7 to −11 μm. Micrographs were digitized in a Nikon Super Coolscan 9000 scanner.

To quantify the morphological differences between leaky HPPH liposomes and stable std. liposomes as well as for the crystals they enclosed, we measured the two major dimensions of the liposomes (a and b) and the crystals (a′ and b′) (Fig. 2B, diagrams on the right). From these measurements the aspect ratio of both the liposomes themselves and those from the enclosed crystals were calculated. Aspect ratios were used to discriminate liposomes and crystals in both samples into brackets defined by the values indicated in the graphs. The number of liposomes or crystals in each bracket was expressed as a percentage of the total number of liposomes (n = 50). Percentages and aspect ratios were plotted as histograms that were fitted to a polynomial function producing the distributions in Fig. 2B (left panel).

2.3. In vitro stability

For serum stability measurements, HPPH liposomes or std. liposomes (~20 mg/mL lipids) were diluted 200 times in PBS containing 50% mature bovine serum (Pel-Freez #37218-5), or 50 mg/mL bovine serum albumin (BSA, AMRESCO #9048-46-8), or 25 mg/mL bovine gamma globulin (BGG, Pel-Freez #27005-1). Initial readings were taken and samples were incubated at 37 °C for 24 h. Triton X-100 was added to 0.25% to lyse the liposomes and final fluorescence values were read. Dox release was calculated according to the formula % Release = $(F_{Final} - F_{initial})/(F_{TX\text{-}100} - F_{initial}) \times 100\%$.

For gel permeation, 50 μL of leaky HPPH liposomes (D:L molar ratio 1:4, Dox 3.5 mg/ml), stable std. liposomes (D:L molar ratio 1:4, Dox 3.5 mg/ml) or an equal amount of free Dox were incubated in 500 μl of 50% bovine serum for 24 h at 37 °C. A 30% acrylamide solution was prepared with Acryl/Bis 19:1 premixed powder (Amresco # 0729); 0.05% ammonium persulfate and 0.05% TEMED were added and the solution was poured into 3.5 cm diameter petri dishes. Gel was polymerized overnight. 50 μL of sample was added to a hole in the center of the gel. Dox fluorescence was imaged with a LUMINA IVIS imager immediately and after 6 h of incubation at room temperature, using 465 nm excitation and a DS-red emission filter.

For ex vivo tumor permeation, MIA Paca-2 tumors from sacrificed mice were removed and incubated with 100 μL leaky HPPH liposomes (3.5 mg/mL Dox), stable std. liposomes (3.5 mg/mL Dox) or an equal amount of free Dox in 2 mL of 100% mature bovine serum for 24 h at 37 °C. The tumor slices were prepared and scanned as described below.

2.4. Pharmacokinetics study

All procedures in this work performed on mice were approved by the University at Buffalo Institutional Animal Care and Use Committee. Female mice (female CD-1, 18–20 g, Charles River) were injected via tail vein with HPPH liposomes or std. liposomes (5 mg/kg or 10 mg/kg Dox) at the indicated D:L loading ratios. Small blood volumes were sampled at sub-mandibular and retro-orbital locations at the indicated time points. Blood was centrifuged at 2000 g for 15 min. 10 μL serum was added to 990 μL extraction buffer (0.075 N HCl, 90% isopropanol) and stored for 20 min at −20 °C. The samples were removed and warmed up to room temperature and centrifuged for 10 min at 10,000 *g*. The supernatants were collected and analyzed by fluorescence. Dox and HPPH (excitation 400 nm and emission 660 nm) concentrations were determined from standard curves. Non-compartmental pharmacokinetics parameters were analyzed by PKsolver [39].

2.5. Tumor deposition of Dox

Five week old female nude mice (Jackson Labs, #007850) were inoculated with 2×10^6 KB cells on both flanks and randomly grouped into 1) leaky HPPH liposomes or 2) stable std. liposomes + empty HPPH liposomes groups when the sizes of the tumors reached 6–8 mm (n = 16 per group). Injection dose for both formulations was 10 mg/kg based on Dox (D:L molar ratio 1:4) and 3.9 mg/kg HPPH lipid. Liposomes were injected via tail-vein and 15 min later, tumors were irradiated for 12.5 min with a light dose of 200 mW/cm^2 from a 665 nm laser diode (RPMC laser, LDX-3115-665). Mice were sacrificed and tumors were collected immediately after irradiation, 0.5 h, 4 h and 24 h after irradiation, n = 4 for each time point. For tumor drug deposition determination and biodistribution study, tumors and indicated organs were collected and homogenated in nuclear lysis buffer [0.25 mol/L sucrose, 5 mmol/L Tris–HCl, 1 mmol/l $MgSO_4$, 1 mmol/L $CaCl_2$ (pH 7.6)] and

extracted overnight in 0.075 N HCl 90% isopropanol. Dox and HPPH-lipid was determined via fluorescence measurements.

2.6. Fluorescence microscopy

Mice treated with leaky HPPH liposomes or (stable std. liposomes + empty HPPH liposomes) with or without laser irradiation were sacrificed 24 h post treatment. Tumors were collected and embedded immediately with OCT compound (VWR # 25608-930) in embedding molds, snap frozen in liquid nitrogen and stored at −80 °C prior to sectioning and fluorescence microscopy. Tumors were sectioned in a cryostat at −20 °C at 10 μm thickness. Fluorescence microscopy for Dox and HPPH was carried out with an EVOS FL Auto microscope with a 20× objective lens. Dox was imaged with filter cubes with 470 nm excitation and 593 nm emission. HPPH-lipid was imaged with a filter cube with 400 nm excitation and 679 nm emission. Whole tumor sections were automatically imaged, stitched, and cropped. For processing, images were downsampled and all contrast was adjusted identically for all images. For region of interest analysis, 5 squares with 1 mm size were randomly placed in the central region of each tumor and histogram values were extracted using ImageJ.

2.7. Tumor growth study

2×10^6 KB cells (Hela subline) or 5×10^6 MIA Paca-2 cells were injected in the right flank female nude mice (5 weeks, Jackson Labs, #007850). When tumors reached 4–6 mm in diameter, mice bearing KB tumors were grouped as follows: 1) Saline control, n = 5; 2) stable std. liposomes, n = 7; 3) stable std. liposomes + empty HPPH liposome with laser, n = 7; 4) Leaky HPPH liposomes with laser, n = 7. Stable std. liposomes were composed of DSPC:PEG:CHOL (60:5:35 by mole, D:L molar ratio 1:5) and an alternative leaky HPPH liposome formulation (1.6 h Dox half-life, unpublished data) composed of DSPC:HPPH-lipid:PEG:CHOL (50:10:5:35 by mole, D:L molar ratio 1:8). Dosage for each formulation was 10 mg/kg Dox and 15.5 mg/kg HPPH-lipid. For mice bearing MIA Paca-2 tumors, the groups were: 1) Saline control, n = 5; 2) Leaky HPPH liposomes without laser, n = 6; 3) stable std. liposomes + empty HPPH liposome with laser, n = 5; 4) Leaky HPPH liposomes with laser, n = 6. Stable std. liposomes was composed of DSPC:PEG:CHOL (50:5:45 by mole, D:L molar ratio 1:4) and leaky HPPH liposomes were composed of DSPC:HPPH-lipid:PEG:CHOL (45:5:5:45 by mole, D:L molar ratio 1:4). Intravenous dosage for each formulation was 10 mg/kg based on Dox and 3.9 mg/kg based on HPPH-lipid.

15 min after tail-vein injection, tumors were irradiated at a fluence rate of 200 mW/cm^2 for 12.5 min. Tumor size was monitored 2–3 times per week and tumor volumes were estimated by measuring three tumor dimensions using a caliper and the ellipsoid formula: Volume $= \pi \cdot L \cdot W^2/6$, where L, W are the length and width of the tumor, respectively. Mice were sacrificed when the tumor grew to five times of its initial volume.

2.8. Statistical analysis

Data were analyzed by Graphpad prism (Version 5.01) software as indicated in figure captions. Differences were considered significant at $P < 0.05$ (*$P < 0.05$, **$P < 0.01$, ***$P < 0.001$).

3. Results

3.1. Tuning liposome leakiness by varying the drug to lipid ratio

HPPH-liposomes with a molar ratio of DSPC:CHOL:PEG2K:HPPH-lipid 45:45:5:5 and standard (std.) liposomes with a molar ratio of DSPC:CHOL:PEG2K 50:45:5 were formed via a hot ethanol injection method. Loaded HPPH liposomes and std. liposomes were generated by loading Dox into the liposomes with an ammonium sulfate gradient [40]. By incubating different amounts of Dox with the liposomes during this step, the drug to lipid ratio could readily be varied. Entrapment efficiencies greater than 90% were achieved for Dox loading into HPPH-liposomes with drug to lipid (D:L) molar ratios ranging from 1:15 to 1:3 (Supporting Fig. 1). When incubated in 50% bovine serum at 37 °C for 24 h, we unexpectedly observed that HPPH liposomes exhibited stability that was dependent on the D:L ratio (Fig. 1A). Lower D:L ratios produced more stable HPPH liposomes. HPPH liposomes with a D:L loading ratio of 1:4 released 60% of the loaded drug, while liposomes with lower D:L ratios reduced the amount of the release to 10%. This is in contrast to std. liposomes, where a 1:4 D:L loading resulted in less than 10% release. Unlike HPPH liposomes, std. liposomes exhibited greater stability with higher D:L ratios which was in accordance with literature [21], although the relation between loading ratio and stability was less pronounced. Even the most destabilized std. liposomes, with a D:L of 1:10 and Dox release of 15%, were significantly more stable than destabilized, leaky HPPH liposomes.

When incubated at 37 °C for 24 h in PBS in the absence of serum, both types of liposomes, with a D:L loading of 1:4, did not release any detectable amount of Dox (Fig. 1B). To determine if proteins found in serum could induce destabilization, HPPH liposomes were incubated with the major serum proteins bovine serum albumin (BSA) and bovine gamma globulin (BGG) at concentrations close to physiological levels. 50 mg/mL BSA induced ~40% Dox release and 25 mg/mL BGG caused ~70% Dox release from leaky HPPH liposomes. The more stable HPPH liposomes (D:L 1:10) and stable std. liposomes exhibited limited drug release when incubated with either type of serum protein. The destabilization of leaky HPPH liposomes by BSA and BGG was dose dependent (Supporting Fig. 2A, 2C). Despite the differences in protein-induced destabilization, when incubated with BSA, the amount of protein absorbed to these three types of liposomes following liposome isolation by gel filtration was similar (Supporting Fig. 2B). Heat inactivated bovine serum (56 °C for 30 min) was not sufficient to prevent destabilization, since drug leakage induced by heat inactivated serum was similar to standard serum (Supporting Fig. 2D). Taken together, these results demonstrate that leaky HPPH liposomes can be destabilized by proteins in serum.

As an indicator of bioavailability, gel permeation of Dox from liposomes with different serum stability was examined. D:L molar ratio of 1:4 was selected for both std. liposomes and HPPH liposomes and are referred to as stable std. liposomes and leaky HPPH liposomes respectively due to their significant difference in serum stability. After incubation with whole bovine serum for 24 h, samples were added to the hole in the center of the gel. As shown in Fig. 1C, the initial Dox florescence in leaky HPPH liposomes group was higher, as a result of Dox being released from leaky HPPH liposomes. 6 h later, the Dox signal covered a significantly higher area than that of Dox-std. group due to the faster penetration rate of free Dox compared to liposomal Dox. We further investigated the tumor penetration of Dox after incubating ex-vivo MIA Paca-2 tumors with stable std. liposomes, leaky HPPH liposomes (Fig. 1D) and free Dox in whole bovine serum for 24 h. Notably, Dox from leaky HPPH liposomes was more homogenously distributed throughout the whole tumor while Dox in stable std. liposomes was restricted to the periphery of the tumor. Additionally, the Dox signal was weak in stable std. liposomes group as Dox was encapsulated and fluorescence was quenched.

3.2. Liposome morphology

The morphology of both stable std. liposomes and leaky HPPH liposomes was analyzed using cryo-transmission electron microscopy. In both Dox-loaded samples, large Dox crystal were enclosed in elongated liposomes while unloaded HPPH liposomes were perfectly spherical (Fig. 2A). This elongated form is different to our previous reports of Dox-loaded HPPH liposomes loaded with lower D:L ratio (1:10),

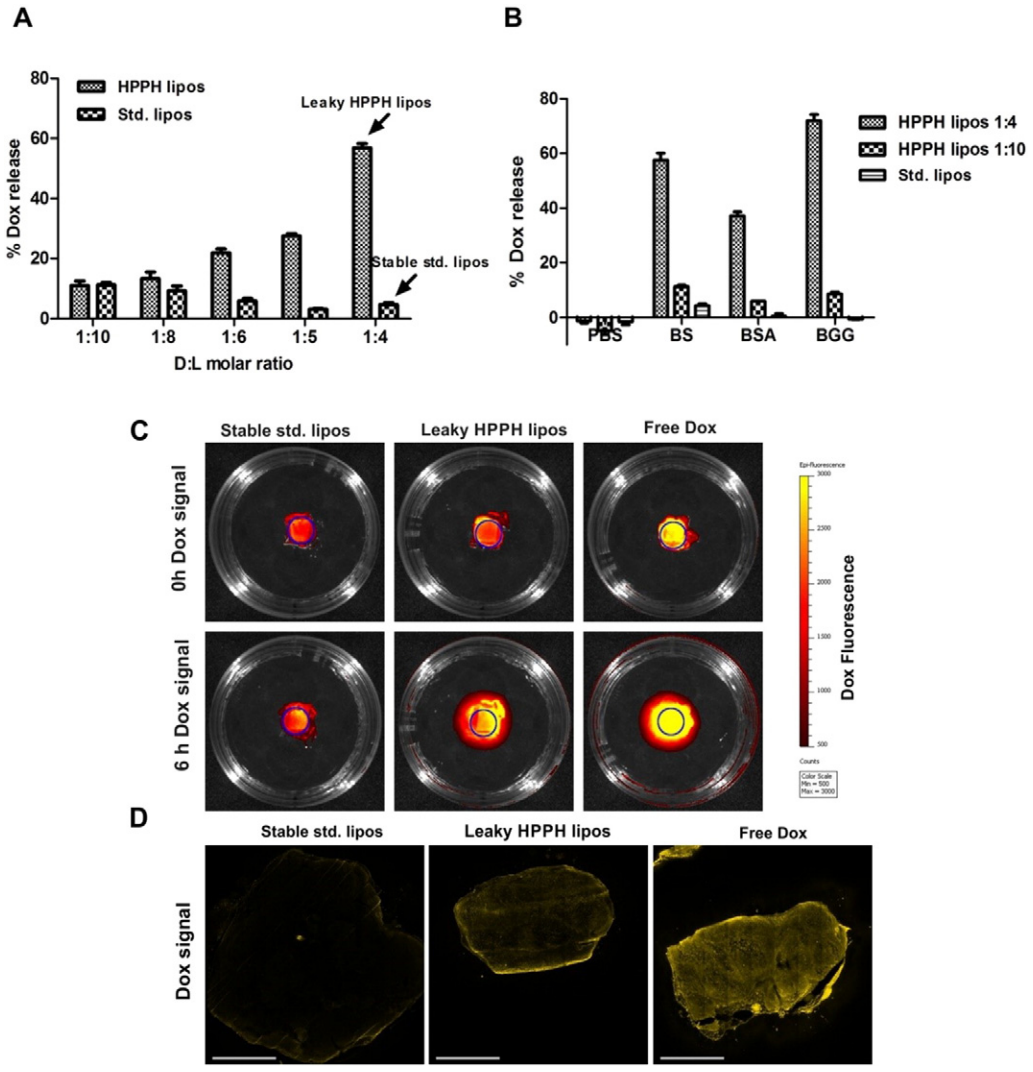

Fig. 1. Controlling Dox release from HPPH liposomes by tuning the drug to lipid ratio. (A) Dox release from HPPH or std. liposomes in 50% bovine serum following 24 h incubation at 37 °C at the indicated drug-to-lipid (D:L) molar ratios. Mean ± S.D. for n = 3. (B) Dox release in PBS, 50 mg/mL bovine serum albumin (BSA), 50% bovine serum (BS) or 25 mg/ml bovine gamma globulin (BGG) following 24 h incubation at 37 °C with indicated liposomes. Mean ± S.D. for n = 3. (C) Permeation of Dox from liposomes pre-incubated with serum in an acrylamide gel. Site of initial incubation is marked by a circle. The upper panel shows the initial Dox distribution while lower panel shows Dox fluorescence 6 h later. Dox signal in leaky HPPH liposomes group is higher than stable std. liposomes due to unquenching of Dox following release from the liposomes. (D) Dox permeation into tumors ex-vivo. Dox fluorescence is shown for whole MIA Paca-2 tumor micrographs. Tumors were incubated with leaky HPPH liposomes or stable std. liposomes in whole bovine serum for 24 h. Due to the destabilization by serum proteins, Dox from leaky HPPH liposomes penetrated further and reached the center of the tumors, resulting in more homogeneous distribution of Dox in the tumor. A 3 mm scale bar is shown. Representative images for n = 3.

which exhibited spherical morphology [34]. In both the stable std. liposomes and leaky HPPH liposome samples, crystals were large, striated, and filled most of the liposome core. Observation of the electron micrographs revealed morphological differences between the two types of liposomes. Leaky HPPH liposomes were consistently elongated with crystals nearly completely filling their lumen. However, stable std. liposomes constituted a more heterogeneous mixture of elongated and rounded particles and with crystals typically leaving more empty space inside the liposomes, especially in those that were more rounded (Fig. 2A, left panel; black arrows).

To obtain a quantitative estimate of the morphological differences between the stable std. liposomes and leaky HPPH liposomes, we measured the length and width of 50 randomly selected liposomes in each sample and their aspect ratios were calculated. A histogram shows the distribution of the liposomes with respect to their aspect ratio (Fig. 2B, top panel). The distribution of leaky HPPH liposomes was narrow and had larger aspect ratio values (4–5), consistent with the observation on the micrographs showing that most of these liposomes are elongated. Conversely, the distribution of stable std. liposomes was significantly broader with similar percentage of liposomes having aspect ratios ranging from 1 to 4. This result shows that the stable std. liposomes were comprised of a more heterogeneous mixture of elongated and rounded liposomes.

The length and width of the Dox crystals enclosed by both the stable std. and leaky HPPH liposomes was measured. The width of the crystals were similar regardless of the liposomes where they were enclosed. However they broadly differed in their length. To measure how homogeneous in size Dox crystals were in the two types of liposomes, we determine the aspect ratio of 50 enclosed crystals in each liposome sample (Fig. 2B, bottom panel). In standard liposomes, the distribution of values was broad, showing that those crystals had multiple lengths. However, the aspect ratio distribution for the Dox crystals in leaky HPPH liposomes was narrower, unimodal and centered on the values corresponding to the largest aspect ratios of the stable std. liposomes. These results suggest that the Dox crystals in the leaky HPPH liposomes were frequently longer and constituted a more homogeneous formulation. Overall, cryo-electron microscopy analysis showed that compared to stable std. liposomes, leaky HPPH liposomes were more homogenous

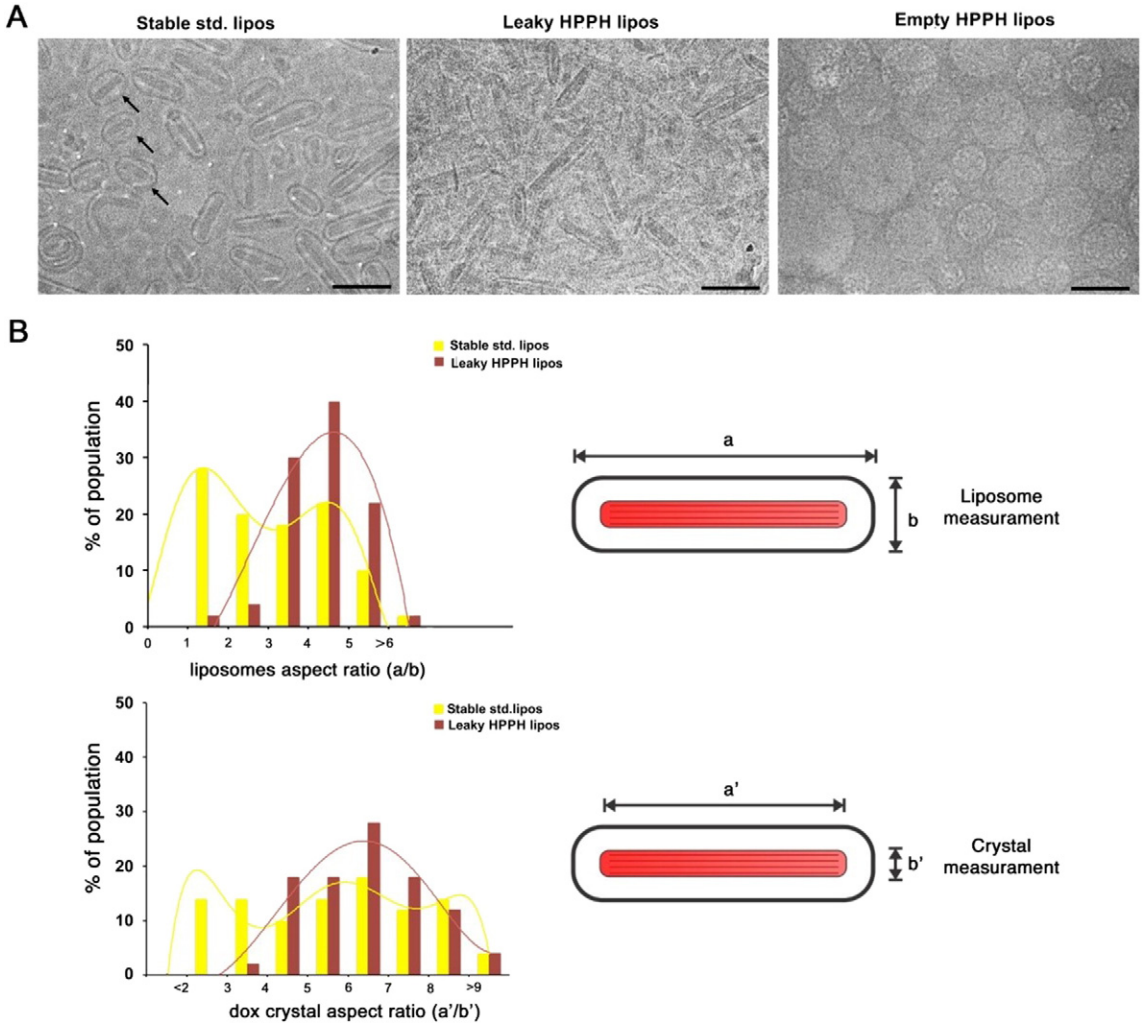

Fig. 2. Morphology of Dox-loaded stable standard and leaky HPPH liposomes with a 1:4 drug-to-lipid ratio. (A) Cryo-electron micrographs of stable std. liposomes (left), leaky HPPH liposomes (middle) and unloaded HPPH liposomes (right). 100 nm scale bars are shown. Black arrows point out some of the more spherical std. liposomes. (B) Distribution of aspect ratios of the liposomes and enclosed Dox crystals, determined as indicated. Histograms for n = 50 were fit with a polynomial function.

in size and shape, and had higher aspect ratios with respect to both the liposomes themselves and the enclosed Dox crystals. The more elongated shape of leaky HPPH liposomes leads to higher membrane curvature at the pointed tips of the liposome. This higher curvature may facilitate protein interaction with the lipid bilayer that leads to destabilization and drug release. In addition, Dox-loaded leaky HPPH liposomes appeared to have a thinner bilayer compared to that of stable std. and empty HPPH liposomes (4 nm vs. 6 nm, Supporting Fig. 3). The thinner bilayer may further facilitate bilayer destabilization of leaky HPPH liposomes by serum proteins.

3.3. Pharmacokinetic parameters

The pharmacokinetic properties of Dox entrapped in various liposomal formulations (5 mg/kg and 10 mg/kg Dox) were assessed. As shown in Fig. 3 and Table 1, HPPH liposomes with lower D:L loading ratio exhibited longer drug blood circulation times, higher areas under the curve (AUC), slower clearance rates and smaller volumes of distribution. At a 10 mg/kg Dox dose, HPPH liposomes with 1:4 D:L loading ratio had the shortest Dox half-life (7.4 h), followed by HPPH liposomes with 1:6 (10.7 h) then 1:8 (12.9 h). Std. liposome formulation used the 1:4 D:L loading ratio exhibited the longest drug circulation of all the formulations assessed. At the same Dox dose, stable std. liposomes had a Dox half-life of 16.6 h and an AUC more than double the 1:8 loaded HPPH liposomes and triple the 1:4 loaded HPPH liposomes. Thus, the *in vitro* serum stability trends were also observed *in vivo*. As shown in Fig. 3B, unlike the entrapped drug, HPPH liposomes themselves all displayed similar and extended blood clearance rates, regardless of the loading ratios. This indicates that HPPH liposomes became destabilized and released Dox, which was rapidly cleared from the blood, while the liposomes themselves continued to circulate. This is supported by the normalized ratio in blood between the Dox and HPPH-lipid, which is shown in Fig. 3C. Over a 24 h period, the 1:4 D:L HPPH liposomes that remained in circulation released the majority of their Dox cargo. Together, these data show that *in vivo* control of pharmacokinetic parameters of the entrapped Dox could be achieved by simply adjusting the D:L ratio in HPPH liposomes. As Dox-loaded leaky HPPH-liposomes had a half-life of 7.4 h (10 mg/kg dose) and the volume of distribution was similar to that of stable std. liposomes (Table 1), leaky HPPH liposomes were presumably still stable enough to avoid toxicity from prematurely Dox release in blood. However, in depth toxicity studies are required before any conclusions about toxicity can be made.

3.4. PDT-induced drug deposition in a dual tumor model

Tumoral drug uptake at different time after laser treatment was assessed. A dual tumor model was used with athymic nude mice bearing a xenograft on each flank. Mice were administered with either leaky HPPH liposomes or empty HPPH liposomes plus stable std. liposomes (10 mg/kg Dox for both groups). 15 min following

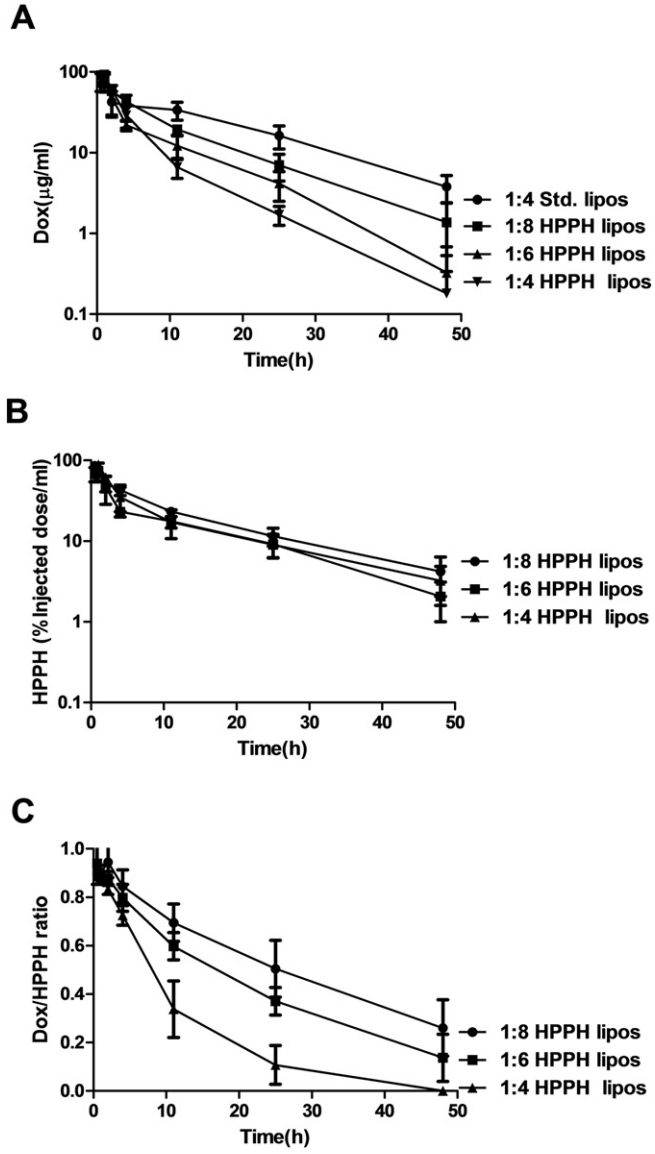

Fig. 3. Blood circulation of liposomes with different drug-to-lipid loading ratios (A) Amount of Dox in blood of mice injected with HPPH liposomes or Std. liposomes at the indicated D:L molar ratio at a Dox dose of 5 mg kg^{-1}; (B) % of injected HPPH dose in 1 ml blood for the same mice used in A. (C) Dox-to-HPPH ratio (% injected dose ratio) for the same mice used in A. Results are mean ± std. dev. for n = 4 mice.

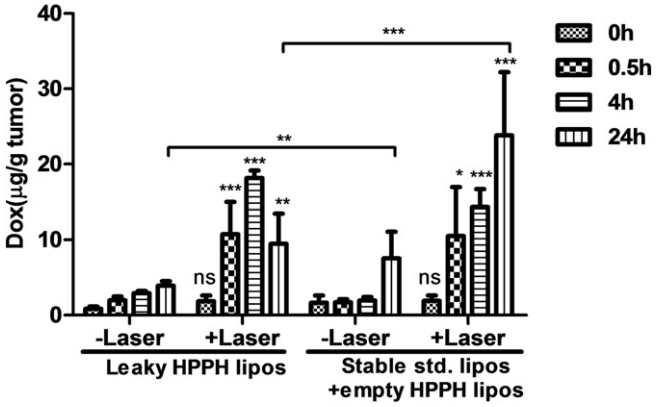

Fig. 4. PDT-induced enhanced Dox deposition in a dual tumor model. Dox deposition in tumors at 0, 0.5, 4 and 24 h after treatment with or without laser irradiation. Asterisks denote significant difference compared with "− laser" group at the corresponding time point, or between leaky HPPH liposomes and stable std. + empty HPPH liposomes at 24 h. Phototreatment significantly enhanced tumor uptake of Dox for both leaky HPPH liposomes and stable std. liposomes groups, except immediately after laser treatment where there is no significant difference between +laser and −laser. At the 24 h time point, Dox deposition from leaky HPPH liposomes group was significantly less than that from stable std. liposomes group both with or without laser treatment ($P < 0.01$). (*$P < 0.05$, **$P < 0.01$, ***$P < 0.001$, all analysis were performed by Bonferroni post-test, two way ANOVA.)

administration, tumors on one flank was irradiated for 12.5 min. Immediately following laser treatment, there was no difference in the amount of Dox deposited in the laser treated tumor compared to the non-irradiated control tumor (Fig. 4). This shows that for this liposome formulation and phototreatment, light-triggered drug release did not drive enhanced Dox uptake into the tumor.

At subsequent time points, laser irradiation led to significantly enhanced Dox deposition (Fig. 4) and HPPH-liposomes uptake for both groups (Supporting Fig. 4A). 30 min following treatment, laser treated tumors form both groups had ~10 μg/g Dox, a ~5 fold increase compared to the untreated tumor. Thus, vascular PDT was sufficient to induce a large enhancement in tumoral drug uptake. 4 h after treatment, drug accumulation increased throughout all tumors, with the irradiated ones maintaining a ~5 fold enhancement tumoral uptake compared to the untreated tumors for both groups. 24 h following treatment, the amount of Dox in the irradiated tumors maintained a ~3 fold enhancement compared to the non-irradiated tumors for both groups. Notably, between the 4 and the 24 h time points, intratumoral Dox levels in the irradiated tumors increased in the stable std. liposome + empty HPPH liposome group but decreased in the leaky HPPH liposome group. This is in accordance with short circulation time of Dox-loaded leaky HPPH liposomes compared with stable std. liposomes (7.4 h versus 16.6 h), as liposomes with longer circulating time will led to more tumor accumulation [8,9]. However, levels of HPPH-lipid did not decrease in either group (Supporting Fig. 4A). The decrease in Dox (but not HPPH-lipid) levels in the tumor suggests that Dox was released in the extracellular space of the tumor, with some of the free Dox subsequently diffusing through the tumor cell membranes but also partially draining out of the tumor.

The distribution of Dox in key organs including heart, liver, spleen, lung and kidney was examined at 0.5 h, 4 h and 24 h (Supporting Fig. 4B, 4C) for both groups. The accumulation of Dox in key organs was

Table 1
Noncompartmental pharmacokinetics analysis of liposomal Dox.

	Dox: 5 mg/kg				Dox: 10 mg/kg			
	HPPH-lipos 1:4	HPPH-lipos 1:6	HPPH-lipos 1:8	Std. lipos 1:4	HPPH lipos 1:4	HPPH lipos 1:6	HPPH lipos 1:8	Std. lipos 1:4
$t_{1/2}$(h)	5.7 ± 3.2	6.9 ± 2.6	9.3 ± 2.2	11.6 ± 0.9	7.4 ± 5.8	10.7 ± 2.4	12.9 ± 1.3	16.6 ± 5.2
C_{max} (μg/ml)	94.2 ± 4.8	82.5 ± 21.1	92.6 ± 4.6	88.7 ± 7.5	216.2 ± 11.6	217.7 ± 35.2	237.2 ± 17.8	278.3 ± 57.7
$AUC_{0\to\infty}$ (μg·h/ml)	415 ± 57	462 ± 75	739 ± 127	1075 ± 299	1331 ± 293	1730 ± 326	2563 ± 209	5764 ± 1714
$MRT_{0\to\infty}$ (h)	5.5 ± 2	8.9 ± 1.4	11.5 ± 2.6	17.4 ± 1.1	6.8 ± 3	10.4 ± 0.4	14.4 ± 1.4	22.7 ± 6.2
Cl (ml/h/g)	0.024 ± 0.003	0.022 ± 0.004	0.014 ± 0.002	0.01 ± 0.002	0.008 ± 0.001	0.006 ± 0.001	0.004 ± 0	0.002 ± 0.001
V_{ss} (ml/g)	0.13 ± 0.03	0.19 ± 0	0.15 ± 0.01	0.17 ± 0.04	0.05 ± 0.01	0.06 ± 0.01	0.06 ± 0	0.04 ± 0

Drug to lipid molar ratios are indicated. Values shown represent mean ± std. dev. for n = 4. MRT; median residence time. AUC; the area under the product of c · t plotted against t from time 0 to infinity. Cl, clearance. V_{ss}, volume of distribution at steady state.

similar to that of stable std. liposomes. The absence of light-triggered release induced Dox accumulation was further verified by separating PDT and light triggered release effect on Dox tumoral accumulation (Supporting Fig. 4D). After PDT treatment with empty HPPH liposomes, mice were injected with Dox-loaded leaky HPPH liposomes, so any enhancement of Dox accumulation could unambiguously be attributed to PDT effect. Since there was no significant difference in tumor uptake between this treatment and the normal treatment procedure (injection of Dox-loaded leaky HPPH liposomes followed by laser treatment), we concluded that the impact from light triggered release was minimal.

3.5. Spatial distribution of tumoral Dox and HPPH

Since both Dox and HPPH-lipid are fluorescent, they could be directly visualized within tumors (Fig. 5A). 24 h after treatment, tumors were excised, frozen, sectioned and imaged with fluorescence microscopy. Whole tumor slices were visualized using automated image collection and micrograph stitching. Most of Dox and HPPH-lipid were localized at the peripheral boundary of the tumors. Little Dox reached the central core of the tumors, with the exception of the tumors laser treated in the leaky HPPH liposome group. For those, a more uniform spatial distribution of Dox in tumors was observed, suggesting a considerable amount of Dox leaked out of the liposomes and became bioavailable to a greater portion of the tumor, not just the periphery. The liposomes themselves were not as uniformly distributed. As shown in Supporting Fig. 5, co-localization of Dox and HPPH-lipid was observed for stable std. liposomes + empty HPPH liposome group, showing that two types of co-injected liposomes extravasated to the same location, that Dox did not diffuse out of the liposomes, and that liposomes did not diffuse far into the tumor. This same pattern for std. liposomes was also observed in the irradiated tumors, although the amount of deposited HPPH-lipid and Dox were greater. These results are consistent with drug remaining entrapped within the std. liposomes.

To further quantify Dox release in the core of the tumor, the Dox pixel intensities within five randomly selected 1 mm square regions of interest (ROIs) close to the center of the tumor were analyzed. As shown in Fig. 5B, for std. liposomes, only a small fraction of pixels in the ROIs had non-zero values, reflecting the sparsity of the drug. Laser irradiation increased the number of non-zero Dox pixels to ~15%. The non-irradiated tumors from mice treated with leaky HPPH liposomes also had very few non-zero Dox-pixels in the core of the tumor. However, the laser-irradiated samples had ROIs with dramatically higher proportion of non-negative Dox pixels. Approximately 75% of the pixels in the ROIs had Dox pixels with non-zero values. This demonstrates that significantly broader spatial distribution and enhanced bioavailability of leaky HPPH liposomes is achieved following laser irradiation and vascular PDT.

3.6. Anti-tumor efficacy

Given the lower drug concentration at 24 h, but the superior intratumoral spatial biodistribution, anti-tumor phototherapy using leaky HPPH liposomes was compared to stable std. liposomes coinjected with unloaded HPPH liposomes. Nude mice bearing KB tumor were grouped and administered with: 1) saline control; 2) stable std. liposomes; 3) stable std. liposomes + empty HPPH liposomes + laser irradiation; 4) leaky HPPH liposomes + laser irradiation (Table 2). In similar conditions, we previously demonstrated that unloaded HPPH liposomes alone with or without laser treatment are ineffective tumor treatments [34]. As shown in Fig. 6A, tumors in the saline group grew

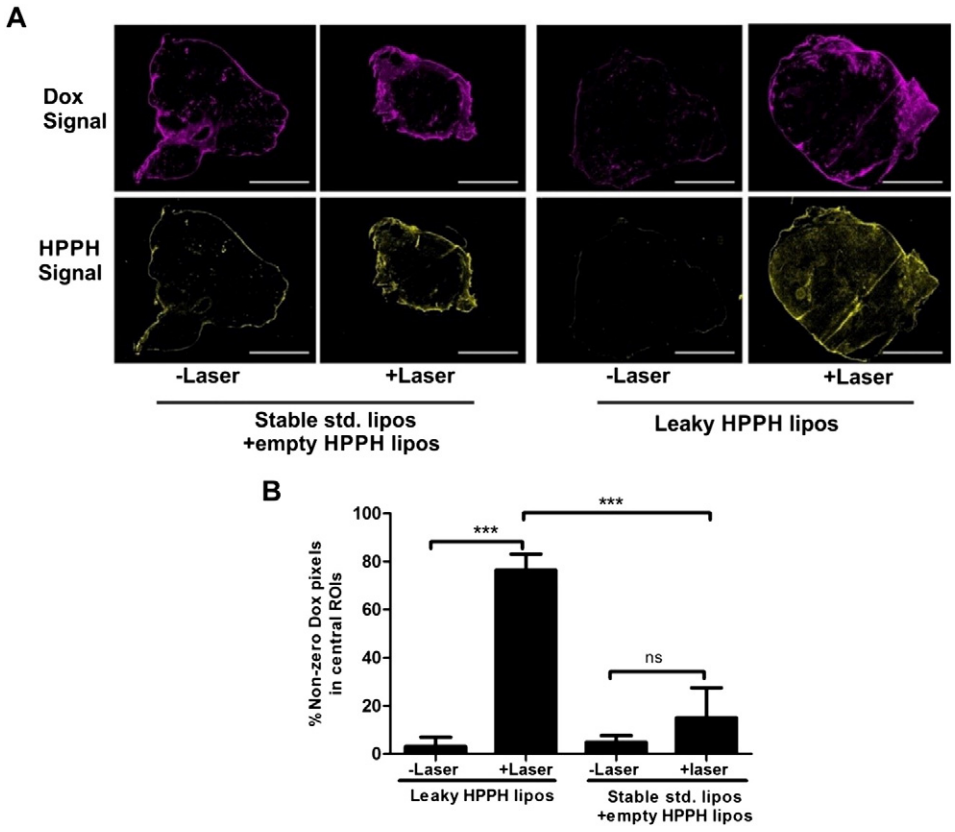

Fig. 5. Dox and HPPH-lipid distribution 24 h after treatment with or without laser irradiation. Following laser irradiation of mice injected with the indicated liposomes (10 mg/kg Dox), mice were sacrificed and tumors were collected 24 h after irradiation. (A) Whole tumor micrographs from mice injected with indicated liposomes with or without laser irradiation. 3 mm scale bars are shown. (B) Five 1 mm square regions of interest were randomly selected close to the center of the tumor and the percentage of non-zero Dox pixels were calculated. Asterisks denote significance. Significant difference of the +laser groups between leaky HPPH liposomes and stable std. liposomes + empty HPPH liposomes was observed. (***$P < 0.01$, Tukey's Multiple Comparison Test, one-way ANOVA).

Table 2
Tumor growth characteristics.

	KB tumors				MIA Paca-2 tumors			
	Saline	Stable std. lipos	Stable std. + empty HPPH lipos + laser	Leaky HPPH lipos + laser	Saline	Leaky HPPH lipos − laser	Stable std. + empty HPPH lipos + laser	Leaky HPPH lipos + laser
Growth days	6.6(0.9)	18.9(5.3)[a]	39.6(9.3)[b]	Cured	15.2(1.6)	18.0(3.0)	Cured	Cured
Growth delay		12.3	33	Cured		2.8	Cured	Cured
Cure rate (%)	0	0	71.4	100.0	0	0	80.0	100.0
Days to regress			17.4(4.3)	15.3(6.5)			21(6.9)	10.2(2)[c]
AUC			33.9(20.9)	16.4(3.5)[d]			22.6(11.4)	7.8(0.8)[e]

Growth days is defined as the days to reach endpoint (five times initial tumor volume). Growth delay was defined as (growth days) − (growth time for saline control). Cure was defined as no tumor present at 45 days (KB tumors) or 33 days (MIA Paca-2 tumors) after treatment. Days to regress was defined as the time required to tumor volume reduces to less than 20 mm^3. AUC was defined as the area of the relative tumor volume of [stable std. + empty HPPH liposomes + laser] and [leaky HPPH liposomes + laser] in the period when all the mice in the former group were alive. Data in the table shows means and values in parentheses represent the std. dev. with n=5-7 mice per group.

[a] Stable std. liposomes alone significantly delayed the growth of KB tumors. (**$P < 0.01$, Tukey's multiple comparison test, one-way ANOVA).

[b] Stable std. liposomes + empty HPPH liposomes + laser group is significantly better than stable std. liposomes alone. (***$P < 0.001$, Tukey's multiple comparison test, one-way ANOVA).

[c,d,e] There is significant difference between [stable std. + empty HPPH liposomes + laser] and [leaky HPPH liposomes + laser] groups (**$P < 0.01$,*$P < 0.05$,*$P < 0.05$, respectively, unpaired t test).

quickly and reached the endpoint (five times the initial volume) within 6.6 days. A single dose of HPPH liposomes moderately delayed tumor growth endpoint for 12.3 days ($P < 0.01$). The laser-treated std. liposomes with empty HPPH liposomes was a more effective treatment compared with std. liposomes alone ($P < 0.001$), and induced a slow tumor cure in 5 out of 7 mice. However, for the leaky HPPH liposomes, tumors shrank more quickly and all of the tumors were cured. When comparing the area under the relative tumor volume, significant difference was observed between leaky HPPH liposomes + laser and stable std. + empty HPPH liposome group (*$P < 0.05$). Mice body mass were monitored and demonstrated no weight loss in the treated groups (data not shown).

Another tumor model with nude mice bearing MIA Paca-2 xenografts were used to further compare the anti-tumor efficacy of leaky HPPH liposomes and stable std. liposomes + empty. Faster and more effective tumor eradication was observed for leaky HPPH liposomes + laser group. As shown in Fig. 6B, it took 21 days for tumors in stable std. liposomes + empty HPPH liposomes group to regress to less than 20 mm^3 and only 10.2 days for Dox-HPPH group (**$P < 0.01$). Significant difference was observed between these two groups when comparing the area under the relative tumor volume (*$P < 0.05$). Thus, despite the higher amount of Dox deposited by stable Std. liposomes in irradiated tumors, the fact that Dox remained trapped inside the liposomes and was not as bioavailable as HPPH liposomes can be the reason that this treatment did not induce rapid tumor regression. Notably, there was no significant difference between saline group and leaky HPPH liposomes without laser treatment group ($P = 0.11$). This can be attributed to instability of leaky HPPH liposomes which leads to less Dox tumor deposition when used alone. Leaky HPPH liposomes with laser irradiation constituted the most effective anti-tumor treatment.

4. Discussion and conclusions

Liposomal doxorubicin, vincristine and topotecan have been shown to have longer blood circulation times when loaded at higher D:L ratios. [21–23] However, HPPH liposomes demonstrate the opposite phenomenon, where higher D:L ratios resulted in faster Dox release in serum *in vitro* and *in vivo*. The mechanism of destabilization in HPPH liposomes is therefore distinct. The only formulation difference between std. liposomes and HPPH liposomes was the replacement of 5 molar % of DSPC with HPPH-lipid, and therefore it appears that serum components interacted with the HPPH-lipid to induce the destabilization, given the stability of the formulation in PBS (Fig. 1B). Serum components such as BGG and BSA dose dependently destabilized the leaky HPPH liposomes (D:L molar ratio 1:4), to a much less degree to that of stable HPPH liposomes (D:L molar ratio 1:10) (Fig. 1B and Supporting Fig. 2A, 2B). Other proteins including high density lipoproteins may destabilize leaky HPPH liposomes as it has been shown that these serum components can bind onto the liposome surface and causes disintegration of liposomes. [41–44] Bovine serum devoid of complement function by heat inactivation destabilized leaky HPPH liposome to the same degree as normal bovine serum (Supporting Fig. 2C). Cryo-TEM in Fig. 2 revealed higher aspect ratios in leaky HPPH liposomes, so regions of high membrane curvature in the elongated liposomes with higher D:L ratios may have facilitated HPPH-lipid exposure to serum proteins which induced leakage. Protein binding to membranes has been reported to, in some cases, be related to membrane curvature [45,46]. However, no quantitative differences were found in BSA binding between stable std. and leaky HPPH liposomes (Supporting Fig. 2B) and furthermore populations of high curvature were also observed in stable std. liposomes (Fig. 2). Dox-loaded HPPH leaky liposomes appeared to have a thinner bilayer which may further facilitate the attack from serum proteins which ultimately destabilized Dox-loaded HPPH liposomes (Supporting Fig. 3). Further research is required to understand the mechanism of serum and protein-induced leaky HPPH liposome destabilization.

The dominant factor in this particular treatment appears to be vascular damage followed by enhanced Dox bioavailability from deposited liposomes. As shown in Fig. 4, 30 min to 24 h following laser irradiation, Dox tumor deposition from both leaky HPPH liposomes and stable std. + empty HPPH liposomes groups were significantly enhanced. A single treatment of stable std. liposomes at 10 mg/kg Dox only delayed the tumor growth for 12 days and no cures occurred. However, in combination with vascular PDT, the therapeutic effect was enhanced due to enhanced Dox deposition and additional or synergistic anti-tumor effect from vascular PDT [47–50]. Despite the lower amounts of Dox retained in the tumor for leaky HPPH liposomes at 24 h time point, more effectively and completely eradication of KB tumors were demonstrated compared with the stable formulation std. liposomes. This can be attributed to the improved bioavailability of the drug and more uniform Dox spatial distribution within the tumors (Fig. 5 and Supporting Fig. 5).

Instantaneous PDT-induced enhanced deposition of stable std. liposomes or leaky HPPH liposomes in the tumor during light treatment was negligible. As shown in Fig. 4, immediately after laser treatment, Dox tumor uptake from both leaky HPPH liposomes and stable std. liposomes + empty HPPH liposomes groups were low and there was no significant difference between these two groups and the corresponding non-irradiated tumors. Given the low amount of Dox in the tumor immediately after laser irradiation we concluded there was negligible light-triggered drug release in this treatment. The fact that administration of stand liposomes after tumor vasculature permeabilized with empty HPPH liposomes upon illumination resulted in similar drug accumulation further verified the limited role of light triggered drug release. Slow light release rate of this particular formulation can be the main

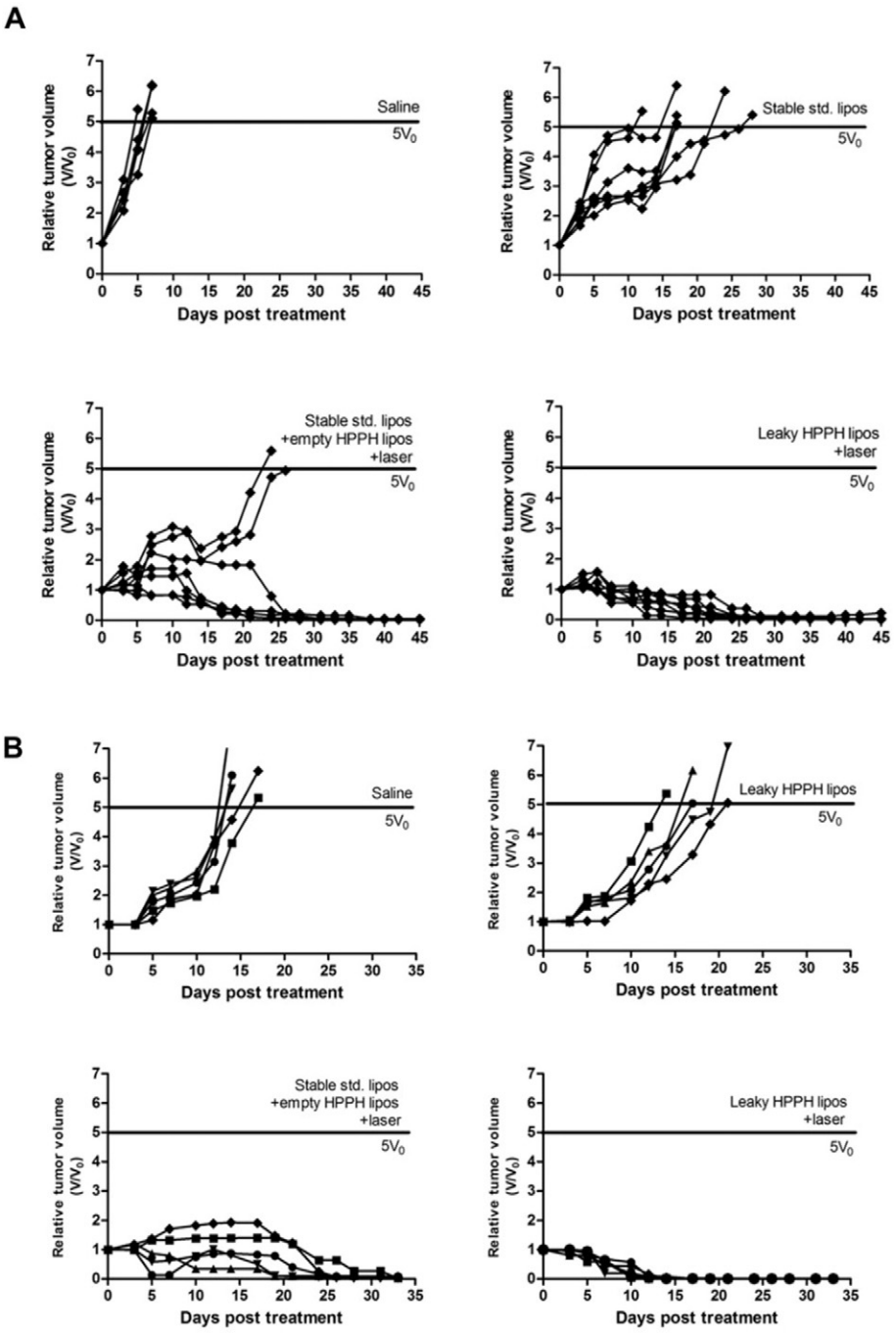

Fig. 6. Complete and rapid tumor eradication with a single phototreatment using Dox-loaded HPPH liposomes. (A) individual tumor growth of nude mice inoculated with KB tumors, treated with saline control; stable std. liposomes alone; stable std.-liposomes + empty HPPH + laser; or HPPH liposomes + laser at a dose of 10 mg/kg of Dox. (B) Individual tumor growth of nude mice inoculated with MIA Paca-2 tumors with saline control, leaky HPPH liposomes without laser, stable std. + empty HPPH liposomes with laser and leaky HPPH liposomes with laser at a dose of 10 mg/kg Dox. Empty HPPH liposome dosage was adjusted to be equivalent with Dox-loaded HPPH liposomes in analogous groups. n = 5–7 per group.

reason for the very limited light release. ~20 min was required for leaky HPPH liposome to release 90% of their contents in bovine serum (Supporting Fig. 6A). Since the entire photo-treatment time was only 12.5 min, only a limited number of liposomes would pass through the tumor and became permeabilized. We did not pursue longer treatment time due to PDT-induced swelling on the treated area. However, we note that both vascular PDT damage and light-induced release parameters of HPPH liposomes are dependent on the formulation and therefore a different liposome formulation, longer laser exposure time or higher laser power may lead to more pronounced light-triggered drug release. The laser triggered release of more stable HPPH liposomes (drug to lipid molar ratio 1:6, 1:8 and 1:10, Supporting Fig. 6B) were further studied. The results indicated that there was no significance in the light triggered release rate of HPPH liposomes of different serum stability. As higher injected amounts of HPPH-lipid can significantly increase the PDT induced side effects, HPPH liposomes with a D:L molar ratio of 1:4 allow for minimized HPPH-lipid use.

Exposure to laser irradiation for varying amounts of time also led to liposome destabilization, resulting in accelerated release of Dox from leaky HPPH liposomes. As shown in Supporting Fig. 6C, laser irradiation for 250 s released less than 15% of liposome contents, however, the release continued to occur once the laser was off, reaching a maximal of

around 70% after 2 h. This could enhance the bioavailability of the fraction of Dox-loaded in leaky HPPH liposomes that get exposed to irradiation. Further studies are required to determine what fraction of liposomes in circulation are exposed to the laser.

In conclusion, Dox release from HPPH liposomes could be controlled *in vitro* and *in vivo* simply by varying the drug to lipid ratio. This strategy was used in conjunction with vascular PDT to enhance the uniformity of drug deposition in tumors. HPPH liposomes induced vascular damage to improve the tumor uptake of the liposomal drug, and the controlled leakiness of HPPH liposomes led to improved bioavailability and better spatial distribution of Dox which ultimately resulted in complete and rapid eradication of subcutaneous tumor xenographs in mice.

Acknowledgments

This work was supported by the National Institutes of Health (R21EB019147, R01EB017270, and DP5OD017898).

Appendix A. Supplementary data

Supplementary data to this article can be found online at http://dx.doi.org/10.1016/j.jconrel.2015.11.011.

References

[1] D. Peer, J.M. Karp, S. Hong, O.C. Farokhzad, R. Margalit, R. Langer, Nanocarriers as an emerging platform for cancer therapy, Nat. Nanotechnol. 2 (2007) 751–760, http://dx.doi.org/10.1038/nnano.2007.387.
[2] V.P. Torchilin, Recent advances with liposomes as pharmaceutical carriers, Nat. Rev. Drug Discov. 4 (2005) 145–160, http://dx.doi.org/10.1038/nrd1632.
[3] F. Szoka, D. Papahadjopoulos, Comparative properties and methods of preparation of lipid vesicles (liposomes), Annu. Rev. Biophys. Bioeng. 9 (1980) 467–508, http://dx.doi.org/10.1146/annurev.bb.09.060180.002343.
[4] Y. Barenholz, Doxil® — the first FDA-approved nano-drug: lessons learned, J. Control. Release 160 (2012) 117–134, http://dx.doi.org/10.1016/j.jconrel.2012.03.020.
[5] E. Rivera, V. Valero, F.J. Esteva, L. Syrewicz, M. Cristofanilli, Z. Rahman, et al., Lack of activity of stealth liposomal doxorubicin in the treatment of patients with anthracycline-resistant breast cancer, Cancer Chemother. Pharmacol. 49 (2002) 299–302.
[6] M.E.R. O'Brien, N. Wigler, M. Inbar, R. Rosso, E. Grischke, A. Santoro, et al., Reduced cardiotoxicity and comparable efficacy in a phase III trial of pegylated liposomal doxorubicin HCl (CAELYX™/Doxil®) versus conventional doxorubicin for first-line treatment of metastatic breast cancer, Ann. Oncol. 15 (2004) 440–449, http://dx.doi.org/10.1093/annonc/mdh097.
[7] K.M. Laginha, S. Verwoert, G.J.R. Charrois, T.M. Allen, Determination of doxorubicin levels in whole tumor and tumor nuclei in murine breast cancer tumors, Clin. Cancer Res. 11 (2005) 6944–6949, http://dx.doi.org/10.1158/1078-0432.CCR-05-0343.
[8] A. Gabizon, R. Catane, B. Uziely, B. Kaufman, T. Safra, R. Cohen, et al., Prolonged circulation time and enhanced accumulation in malignant exudates of doxorubicin encapsulated in polyethylene-glycol coated liposomes, Cancer Res. 54 (1994) 987–992.
[9] A. Gabizon, R. Shiota, D. Papahadjopoulos, Pharmacokinetics and tissue distribution of doxorubicin encapsulated in stable liposomes with long circulation times, J. Natl. Cancer Inst. 81 (1989) 1484–1488, http://dx.doi.org/10.1093/jnci/81.19.1484.
[10] A.A. Gabizon, Selective tumor localization and improved therapeutic index of anthracyclines encapsulated in long-circulating liposomes, Cancer Res. 52 (1992) 891–896.
[11] T.M. Allen, P.R. Cullis, Drug delivery systems: entering the mainstream, Science 303 (2004) 1818–1822, http://dx.doi.org/10.1126/science.1095833.
[12] D. Luo, K.A. Carter, J.F. Lovell, Nanomedical engineering: shaping future nanomedicines, Wiley Interdiscip. Rev. Nanomed. Nanobiotechnol. 7 (2015) 169–188, http://dx.doi.org/10.1002/wnan.1315.
[13] C.-J. Chu, F.C. Szoka, pH-sensitive liposomes, J. Liposome Res. 4 (1994) 361–395, http://dx.doi.org/10.3109/08982109409037050.
[14] V.P. Torchilin, F. Zhou, L. Huang, pH-sensitive liposomes, J. Liposome Res. 3 (1993) 201–255, http://dx.doi.org/10.3109/08982109309148213.
[15] G. Kong, G. Anyarambhatla, W.P. Petros, R.D. Braun, O.M. Colvin, D. Needham, et al., Efficacy of liposomes and hyperthermia in a human tumor xenograft model: importance of triggered drug release, Cancer Res. 60 (2000) 6950–6957.
[16] D. Needham, M.W. Dewhirst, The development and testing of a new temperature-sensitive drug delivery system for the treatment of solid tumors, Adv. Drug Deliv. Rev. 53 (2001) 285–305, http://dx.doi.org/10.1016/S0169-409X(01)00233-2.
[17] R. de la Rica, D. Aili, M.M. Stevens, Enzyme-responsive nanoparticles for drug release and diagnostics, Adv. Drug Deliv. Rev. 64 (2012) 967–978, http://dx.doi.org/10.1016/j.addr.2012.01.002.
[18] C.W. Chang, L. Barber, C. Ouyang, D. Masin, M.B. Bally, T.D. Madden, Plasma clearance, biodistribution and therapeutic properties of mitoxantrone encapsulated in conventional and sterically stabilized liposomes after intravenous administration in BDF1 mice, Br. J. Cancer 75 (1997) 169–177.
[19] H.J. Lim, D. Masin, T.D. Madden, M.B. Bally, Influence of drug release characteristics on the therapeutic activity of liposomal mitoxantrone, J. Pharmacol. Exp. Ther. 281 (1997) 566–573.
[20] G. Adlakha-Hutcheon, M.B. Bally, C.R. Shew, T.D. Madden, Controlled destabilization of a liposomal drug delivery system enhances mitoxantrone antitumor activity, Nat. Biotechnol. 17 (1999) 775–779, http://dx.doi.org/10.1038/11710.
[21] M.J.W. Johnston, K. Edwards, G. Karlsson, P.R. Cullis, Influence of drug-to-lipid ratio on drug release properties and liposome integrity in liposomal doxorubicin formulations, J. Liposome Res. 18 (2008) 145–157, http://dx.doi.org/10.1080/08982100802129372.
[22] M.J.W. Johnston, S.C. Semple, S.K. Klimuk, K. Edwards, M.L. Eisenhardt, E.C. Leng, et al., Therapeutically optimized rates of drug release can be achieved by varying the drug-to-lipid ratio in liposomal vincristine formulations, Biochim. Biophys. Acta Biomembr. 1758 (2006) 55–64, http://dx.doi.org/10.1016/j.bbamem.2006.01.009.
[23] S.A. Abraham, K. Edwards, G. Karlsson, N. Hudon, L.D. Mayer, M.B. Bally, An evaluation of transmembrane ion gradient-mediated encapsulation of topotecan within liposomes, J. Control. Release 96 (2004) 449–461, http://dx.doi.org/10.1016/j.jconrel.2004.02.017.
[24] R.K. Jain, T. Stylianopoulos, Delivering nanomedicine to solid tumors, Nat. Rev. Clin. Oncol. 7 (2010) 653–664, http://dx.doi.org/10.1038/nrclinonc.2010.139.
[25] J. Fang, H. Nakamura, H. Maeda, The EPR effect: unique features of tumor blood vessels for drug delivery, factors involved, and limitations and augmentation of the effect, Adv. Drug Deliv. Rev. 63 (2011) 136–151, http://dx.doi.org/10.1016/j.addr.2010.04.009.
[26] H. Maeda, Tumor-selective delivery of macromolecular drugs via the EPR effect: background and future prospects, Bioconjug. Chem. 21 (2010) 797–802, http://dx.doi.org/10.1021/bc100070g.
[27] H. Maeda, Y. Matsumura, EPR effect based drug design and clinical outlook for enhanced cancer chemotherapy, Adv. Drug Deliv. Rev. 63 (2011) 129–130, http://dx.doi.org/10.1016/j.addr.2010.05.001.
[28] C. He, P. Agharkar, B. Chen, Intravital microscopic analysis of vascular perfusion and macromolecule extravasation after photodynamic vascular targeting therapy, Pharm. Res. 25 (2008) 1873, http://dx.doi.org/10.1007/s11095-008-9604-5.
[29] B. Chen, B.W. Pogue, J.M. Luna, R.L. Hardman, P.J. Hoopes, T. Hasan, Tumor vascular permeabilization by vascular-targeting photosensitization: effects, mechanism, and therapeutic implications, Clin. Cancer Res. 12 (2006) 917–923, http://dx.doi.org/10.1158/1078-0432.CCR-05-1673.
[30] T. Araki, K. Ogawara, H. Suzuki, R. Kawai, T. Watanabe, T. Ono, et al., Augmented EPR effect by photo-triggered tumor vascular treatment improved therapeutic efficacy of liposomal paclitaxel in mice bearing tumors with low permeable vasculature, J. Control. Release 200 (2015) 106–114, http://dx.doi.org/10.1016/j.jconrel.2014.12.038.
[31] J.W. Snyder, W.R. Greco, D.A. Bellnier, L. Vaughan, B.W. Henderson, Photodynamic therapy a means to enhanced drug delivery to tumors, Cancer Res. 63 (2003) 8126–8131.
[32] Z. Zhen, W. Tang, Y.-J. Chuang, T. Todd, W. Zhang, X. Lin, et al., Tumor vasculature targeted photodynamic therapy for enhanced delivery of nanoparticles, ACS Nano 8 (2014) 6004–6013, http://dx.doi.org/10.1021/nn501134q.
[33] M. Ethirajan, Y. Chen, P. Joshi, R.K. Pandey, The role of porphyrin chemistry in tumor imaging and photodynamic therapy, Chem. Soc. Rev. 40 (2011) 340–362, http://dx.doi.org/10.1039/B915149B.
[34] K.A. Carter, S. Shao, M.I. Hoopes, D. Luo, B. Ahsan, V.M. Grigoryants, et al., Porphyrin–phospholipid liposomes permeabilized by near-infrared light, Nat. Commun. 5 (2014)http://dx.doi.org/10.1038/ncomms4546.
[35] D. Luo, K.A. Carter, A. Razi, J. Geng, S. Shao, D. Giraldo, et al., Doxorubicin encapsulated in stealth liposomes conferred with light-triggered drug release, Biomaterials 75 (2016) 193–202, http://dx.doi.org/10.1016/j.biomaterials.2015.10.027.
[36] S. Shao, J. Geng, H.A. Yi, S. Gogia, S. Neelamegham, A. Jacobs, et al., Functionalization of cobalt porphyrin–phospholipid bilayers with his-tagged ligands and antigens, Nat. Chem. 7 (2015) 438–446, http://dx.doi.org/10.1038/nchem.2236.
[37] J. Rieffel, F. Chen, J. Kim, G. Chen, W. Shao, S. Shao, et al., Hexamodal imaging with porphyrin-phospholipid-coated upconversion nanoparticles, Adv. Mater. 27 (2015) 1785–1790, http://dx.doi.org/10.1002/adma.201404739.
[38] J.F. Lovell, C.S. Jin, E. Huynh, H. Jin, C. Kim, J.L. Rubinstein, et al., Porphysome nanovesicles generated by porphyrin bilayers for use as multimodal biophotonic contrast agents, Nat. Mater. 10 (2011) 324–332, http://dx.doi.org/10.1038/nmat2986.
[39] Y. Zhang, M. Huo, J. Zhou, S. Xie, PKSolver: an add-in program for pharmacokinetic and pharmacodynamic data analysis in Microsoft Excel, Comput. Methods Prog. Biomed. 99 (2010) 306–314, http://dx.doi.org/10.1016/j.cmpb.2010.01.007.
[40] G. Haran, R. Cohen, L.K. Bar, Y. Barenholz, Transmembrane ammonium sulfate gradients in liposomes produce efficient and stable entrapment of amphipathic weak bases, Biochim. Biophys. Acta Biomembr. 1151 (1993) 201–215, http://dx.doi.org/10.1016/0005-2736(93)90105-9.
[41] T.M. Allen, L.G. Cleland, Serum-induced leakage of liposome contents, Biochim. Biophys. Acta Biomembr. 597 (1980) 418–426, http://dx.doi.org/10.1016/0005-2736(80)90118-2.
[42] Z. Panagi, K. Avgoustakis, G. Evangelatos, D.S. Ithakissios, In vitro binding of HSA, IgG, and HDL on liposomes of different composition and its correlation with the BLOOD/RES ratio of liposomes, Int. J. Pharm. 176 (1999) 203–207, http://dx.doi.org/10.1016/S0378-5173(98)00315-9.
[43] G. Scherphof, F. Roerdink, M. Waite, J. Parks, Disintegration of phosphatidylcholine liposomes in plasma as a result of interaction with high-density lipoproteins, Biochim. Biophys. Acta Gen. Subj. 542 (1978) 296–307, http://dx.doi.org/10.1016/0304-4165(78)90025-9.

[44] J. Zborowski, F. Roerdink, G. Scherphof, Leakage of sucrose from phosphatidylcholine liposomes induced by interaction with serum albumin, Biochim. Biophys. Acta Gen. Subj. 497 (1977) 183–191, http://dx.doi.org/10.1016/0304-4165(77)90151-9.
[45] V.K. Bhatia, N.S. Hatzakis, D. Stamou, A unifying mechanism accounts for sensing of membrane curvature by BAR domains, amphipathic helices and membrane-anchored proteins, Semin. Cell Dev. Biol. 21 (2010) 381–390, http://dx.doi.org/10.1016/j.semcdb.2009.12.004.
[46] O.G. Mouritsen, Lipids, curvature, and nano-medicine, Eur. J. Lipid Sci. Technol. 113 (2011) 1174–1187, http://dx.doi.org/10.1002/ejlt.201100050.
[47] P.A. Cowled, L. Mackenzie, I.J. Forbes, Potentiation of photodynamic therapy with haematoporphyrin derivatives by glucocorticoids, Cancer Lett. 29 (1985) 107–114, http://dx.doi.org/10.1016/0304-3835(85)90130-2.
[48] E.S. Edell, D.A. Cortese, Combined effects of hematoporphyrin derivative phototherapy and adriamycin in a murine tumor model, Lasers Surg. Med. 8 (1988) 413–417, http://dx.doi.org/10.1002/lsm.1900080413.
[49] M.Y. Nahabedian, R.A. Cohen, M.F. Contino, T.M. Terem, W.H. Wright, M.W. Berns, et al., Combination cytotoxic chemotherapy with cisplatin or doxorubicin and photodynamic therapy in murine tumors1, J. Natl. Cancer Inst. 80 (1988) 739–743, http://dx.doi.org/10.1093/jnci/80.10.739.
[50] G. Canti, A. Nicolin, R. Cubeddu, P. Taroni, G. Bandieramonte, G. Valentini, Antitumor efficacy of the combination of photodynamic therapy and chemotherapy in murine tumors, Cancer Lett. 125 (1998) 39–44, http://dx.doi.org/10.1016/S0304-3835(97)00502-8.